https://doi.org/10.15407/ujpe65.11.1022

V.V. POZHIVATENKO

V.O. Sukhomlynskyi National University of Mykolayiv
(24, Nikols'ka Str., Mykolayiv 54030, Ukraine; e-mail: pozhivatenko@ukr.net)

IONIC CHARACTER, PHASE TRANSITIONS, AND METALLIZATION IN ALKALINE-EARTH METAL OXIDES AND CHALCOGENIDES UNDER PRESSURE

The structural and thermodynamic properties of the alkaline-earth metal oxides and chalcogenides (AEMOCs) with the cubic structure (CaX, SrX, and BaX, where X = O, S, Se, and Te) and the parameters of the pressure-induced B1–B2 structural phase transitions in them have been calculated from the first principles. The crystalline and ionic radii in the AEMOCs are studied including the dependences of the ionic radii in the B1 and B2 structures on the pressure. The magnitudes of interband transitions and the band gaps in the examined compounds are calculated in the framework of the first-principles approach of the density functional theory and using the method of pseudopotential. The first-principles band calculations are carried out to determine the metallization pressures for the researched compounds.

K e y w o r d s: alkaline-earth metal oxides, alkaline-earth metal chalcogenides, phase transitions, metallization.

1. Introduction

A lot of papers have been devoted to the study of the alkaline-earth metal oxides and chalcogenides (AEMOCs), especially those of them which crystallize in the cubic structure. Most of such researches concerned the structural parameters of the AEMOCs and the parameters of the B1–B2 structural phase transition that occurs in them under the action of a pressure. The other characteristics were not calculated so extensively, especially for the MeX compounds, where Me stands for an alkaline-earth metal and X for oxygen or chalcogen. For instance, interband transitions have been studied much more comprehensively in the B1 structure, which is easier to study experimentally, especially at zero pressure. On the other hand, only some theoretical results are mainly known for the high-pressure structure B2. In general, the number of researches of the AEMOCs in the B2 structure at moderate and high pressures is few (there are almost no data on selenides and tellurides).

The cubic AEMOCs MeX, where Me denotes the Ca, Sr, or Ba atom, demonstrate an ionic character in a wide interval of pressures, because they have the ionic crystal structure B1. If the pressure increases, they undergo a structural phase transition into another ionic crystal structure, B2. If the pressure increases further, they lose their ionic character and undergo the metallization.

In many cases, the approaches that are used to calculate the physical properties of the AEMOCs do not allow one to accurately calculate the parameters of their band structure and the related quantities. This fact also concerns the case of cubic modifications of the AEMOCs, which are studied in this work. In particular, the method of density functional theory (DFT) [1], which is widely used in plenty of researches, including this one, distorts the band structure and leads to an underestimation of gap magnitudes and, perhaps, to an underestimation of metallization pressure values.

This work was aimed at the first-principles study of the ionic properties of the AEMOCs with the cu-

bic structures under the pressure, p, action till their metallization. For this purpose, calculations of the structural properties of the B1 and B2 lattices were performed, the B1–B2 structural transition was analyzed, and the corresponding ionic radii at $p = 0$ were determined. By analyzing the volume changes under the pressure, the corresponding changes of ionic radii were found. The band structure parameters for the B1 and B2 lattices and the metallization pressures for the examined compounds were determined.

2. Calculation Technique

The first-principles calculations of the thermodynamic parameters of the AEMOCs with the B1 and B2 cubic structures were carried out in the framework of the DFT formalism making use of the Quantum ESPRESSO software package [2]. In so doing, the exchange-correlation effects were taken into account according to work [3]. Besides that, the ultrasoft Vanderbilt pseudopotential [4] was used for all elements, except for tellurium, for which the Rappe–Rabe–Kaxiras–Joannopoulos pseudopotential [5, 6] was applied.

The results of calculations were fitted to the third-order Birch–Murnaghan equation of state [7]. The Monkhorst–Pack mesh points were used for the integration over the Brillouin zone. Proceeding from the convergence condition for the results obtained that the calculation accuracy for total energies should not be less than 1×10^{-6} Ry, the choices of the Monkhorst–Pack mesh poins were as follows: for CaO, $12 \times 12 \times 12$ for B1 and $16 \times 16 \times 16$ for B2; for CaS, $20 \times 20 \times 20$ (for both structures); for CaSe, $12 \times 12 \times 12$ for B1 and $20 \times 20 \times 20$ for B2; for CaTe, $12 \times 12 \times 12$ for B1 and $28 \times 28 \times 28$ for B2; for SrO, $12 \times 12 \times 12$ for B1 and $16 \times 16 \times 16$ for B2; for SrS, SrSe, and SrTe, $20 \times 20 \times 20$ (for both structures); for BaO, $12 \times 12 \times 12$ (for both structures); for BaS, $20 \times 20 \times 20$ (for both structures); for BaSe, $12 \times 12 \times 12$ for B1 and $16 \times 16 \times 16$ for B2; and for BaTe, $20 \times 20 \times 20$ (for both structures). The cut-off energy for the wave function expansion was $E_{\text{cut}} = 200$ Ry, and the cut-off energy for the charge density was put equal to $10E_{\text{cut}}$ in all calculations.

3. Structural Parameters of AEMOCs

There is a large number of works devoted to the study of structural parameters of both the alkaline-earth metals (AEMs) and the AEMOCs. At the early stages of the research of those compounds (in 1970–1980s), MgO and CaO were mainly studied. Empirical and semiempirical methods were often used to calculate physical quantities at that time. In the next years, calculations of physical properties were also made for other AEMOCs, including those possessing noncubic structures. Recently, more complicated AEMOC compounds – namely, Me–Me–X and Me–X–X – have been widely studied.

The appearance and development of first-principles approaches in the framework of the DFT and, later, a possibility to generate first-principles pseudopotentials (norm-conserving at first and ultra-soft afterward) made it possible to substantially develop and supplement the set of standard approaches aimed at determining a broad spectrum of those physical parameters of the elements and compounds that are used in modern calculations of the characteristics of crystalline solids. In this work, a formalism suitable for the DFT and pseudopotential methods was applied. The approaches of this kind are currently well adapted to calculate the structural, mechanical, thermodynamic, electronic, and optical properties of crystals.

In the framework of this approach, the structural properties of the AEMOCs – namely, the parameters of the B1 and B2 structures for calcium, strontium, and barium oxides and chalcogenides – were calculated. They include the equilibrium lattice parameter a_0 and, accordingly, the equilibrium volume V_0, as well as the bulk modulus B_0 and its derivative with respect to the pressure, B_0', for each compound. The results of first-principles calculations are presented in Table 1 and the corresponding experimental results in Table 2 for the sake of their comparison. In other theoretical studies, where different computational techniques were applied, a rather good agreement was reached, in general, between the experimental and theoretical results. In addition to the above-mentioned DFT method (and its various implementations), which uses the plane-wave basis, other methods using the basis of wave functions of predefined types were also applied.

The calculations of the AEMOC properties are characterized by a wide range of approaches from various variants of the Hartree–Fock method to the Monte Carlo and molecular dynamics methods. From the viewpoint of further calculations, the calculation accuracy of structural parameters obtained in those

Table 1. **Calculated equilibrium parameters of AEMOCs in the B1 and B2 structures**

Compound	V_0^{B1}, Å^3	a_0^{B1}, Å	B_0^{B1}, GPa	$B_0'^{B1}$	V_0^{B2}, Å^3	a_0^{B2}, Å	B_0^{B2}, GPa	$B_0'^{B2}$
CaO	28.233	4.834	105.002	4.33	25.305	2.936	106.558	4.29
CaS	46.574	5.715	56.329	4.25	42.428	3.488	59.702	4.05
CaSe	53.086	5.966	47.909	4.08	48.699	3.652	50.703	4.07
CaTe	65.605	6.402	36.664	4.03	60.654	3.929	37.634	4.49
SrO	35.179	5.201	83.885	4.55	30.913	3.138	88.172	4.48
SrS	55.613	6.059	47.599	4.60	49.249	3.665	51.770	4.20
SrSe	62.683	6.306	41.509	4.31	55.854	3.822	46.347	3.82
SrTe	76.034	6.725	32.173	4.13	68.397	4.090	35.356	4.20
BaO	40.741	5.462	68.912	4.09	33.739	3.231	72.577	3.70
BaS	64.304	6.360	42.478	4.20	54.119	3.783	44.657	3.90
BaSe	72.037	6.605	36.342	4.32	61.319	3.943	37.301	4.30
BaTe	86.448	7.019	28.811	4.26	74.494	4.208	31.589	4.10

Table 2. **Experimental equilibrium parameters of AEMOCs in the B1 and B2 structures**

Compound	a_0^{B1}, Å	B_0^{B1}, GPa	$B_0'^{B1}$	a_0^{B2}, Å	B_0^{B2}, GPa	$B_0'^{B2}$	Source
CaO	4.810	111.2	4.2	2.907	130	3.5	[9]
CaS	5.689	64	4.2	3.460	64	4.2	[10]
CaSe	5.916	51	4.2	3.612	51	4.2	[10]
CaTe	6.348	42	4.3	3.932	42	4.3	[10]
SrO	5.16	91.3	4.3				[11]
	5.16	90.6	4.4				[11]
SrS	6.024	58					[12]
SrSe	6.234	45.2	4.5		46.5	4.5	[13]
SrTe	6.659	39.5	5				[14]
BaO	5.539	72	5				[15]
BaS	6.387	39.42			34.02		[16]
		55.1	5.5		21.4	7.8	[17]
BaSe	6.600						[18]
	6.593						[19]
BaTe	7.005	29.4	7.4	4.385	27.5	4.6	[20]

approaches can strongly affect the final parameter values of structural phase transitions. A comparison of the results obtained in this work with experimental ones leads to the conclusion that the calculated lattice constants are in reasonable agreement with the experimental data. The worst results – namely, deviations of 1–1.2% – were obtained for SrSe, SrTe, and BaO. The calculated values for the bulk modulus B_0 are in a worse agreement with the experiment. The corresponding deviations reach 18% for SrS and SrTe, and 13% for CaTe; other deviations do not exceed 8%.

For the B2 structure, there are no experimental data for some examined oxides and chalcogenides. By analyzing the known data for B2, we obtain that the lattice constants were calculated with deviations not exceeding 1%, except for BaTe, for which, on the basis of available data, the deviation equals 4%. There are also noticeable discrepancies for the bulk modulus values. The largest deviation of 32% was found for BaS. Thus, the bulk moduli calculated for the B2 structure correspond much worse to the experimental data.

4. B1–B2 Structural Phase Transition in AEMOCs

The results of first-principles calculations of the structural phase transitions in insulators agree rather well

Table 3. **Calculated parameters of the B1–B2 structural phase transition in AEMOCs**

Compound	$p_{\rm pt}$, GPa	$V_0^{\rm B1}$, Å^3	$a_0^{\rm B1}$, Å	$V_{pt}^{\rm B1}/V_0^{\rm B1}$	$V_0^{\rm B2}$, Å^3	$a_0^{\rm B2}$, Å	$V_{\rm pt}^{\rm B2}/V_0^{\rm B1}$	$V_{\rm pt}^{\rm B2}/V_{\rm pt}^{\rm B1}$	ΔV_1, %	ΔV_2, %
CaO	65.238	20.639	4.354	0.731	18.526	2.646	0.656	0.898	7.49	10.24
CaS	36.103	33.837	5.134	0.727	30.898	3.138	0.663	0.913	6.31	8.69
CaSe	33.509	37.585	5.317	0.708	34.871	3.267	0.657	0.928	5.11	7.22
CaTe	29.190	45.146	5.652	0.688	42.736	3.496	0.651	0.947	3.67	5.34
SrO	37.146	27.388	4.785	0.779	24.237	2.894	0.689	0.885	8.97	11.52
SrS	17.812	44.345	5.619	0.797	39.604	3.409	0.712	0.893	8.52	10.69
SrSe	15.549	49.795	5.840	0.794	44.808	3.552	0.715	0.900	7.96	10.02
SrTe	12.348	60.087	6.217	0.790	54.830	3.799	0.721	0.913	6.92	8.75
BaO [a]	13.026	35.374	5.211	0.868	29.362	3.085	0.721	0.830	14.76	17.00
BaS	6.536	57.050	6.111	0.887	48.163	3.638	0.749	0.844	13.82	15.58
BaSe	5.8165	63.720	6.340	0.885	54.368	3.788	0.755	0.853	12.98	14.68
BaTe	4.6325	76.404	6.736	0.884	66.360	4.049	0.768	0.869	11.62	13.15

[a]For a hypothetical B1–B2 phase transition.

Table 4. **Experimental parameters of the B1–B2 structural phase transition in AEMOCs**

Compound	$p_{\rm pt}$, GPa	$V_{\rm pt}^{\rm B1}$, Å^3	$V_{\rm pt}^{\rm B1}/V_0^{B1}$	$V_{\rm pt}^{\rm B2}$, Å^3	$V_{\rm pt}^{B2}/V_0^{B1}$	ΔV_1,%	ΔV_2,%	Source
CaO	63	20.7	0.744	18.7	0.672	7.2	10	[21]
	60–70	20.65–20.22		18.43–18.11			11	[22]
CaS	40		0.73				10.2	[10]
CaSe	38.0	36.26	0.70				7.7	[10]
CaTe	33.0	47.37	0.74			4.6		[10]
	35		0.703				10.8	[14]
SrO	36	27.5	0.815	24.1	0.714	10	13	[23]
SrS	18	44.57	0.815	39.49			11.4	[12]
SrSe	14	49.28	0.813	44.00			10.7	[13]
SrTe	12	60.62	0.828	53.89			11.1	[14]
BaS	6.5		0.917		0.75	16.5	18.2	[17]
	6.5	58.35	0.91	50.37	0.785	12.5	13.7	[16]
BaSe	6						13.9	[19]
BaTe	4.8						13.2	[20]

with the experimental data. The DFT method is known to be able to substantially distort the band structure. Nevertheless, the structural properties of insulators are described rather well. This fact may probably be explained as follows. The results obtained for insulators, unlike those for metals, are little affected by the levels located close to the Fermi one, i.e. the valence band top is separated from the conduction band bottom by a gap that does not introduce additional problems when calculating sums over the occupied states. It is also not excluded that distortions in the band structure of both the B1 and B2 phases change identically with the pressure, which obscures the problem of band energies in the DFT and allows good results for the parameters of the B1–B2 phase transition in the AEMOCs to be obtained.

In this work, the following parameters were calculated for the B1 and B2 structures of the AEMOCs (see Table 3): the phase transition pressure $p_{\rm pt}$, the lattice parameter $a_{\rm pt}$ and the unit cell volume $V_{\rm pt}$ at the phase transition point, the ratio $V_{\rm pt}/V_0$ between $V_{\rm pt}$ and the equilibrium unit cell volume in the B1 structure, and the relative unit cell volume reductions

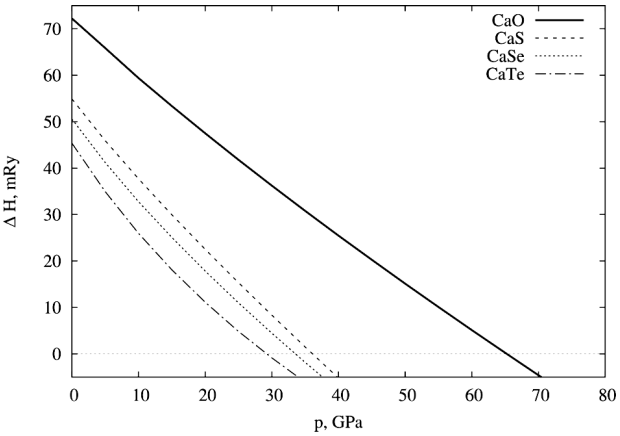

Fig. 1. Dependences of the enthalpy difference between calcium oxide and calcium chalcogenides on the pressure

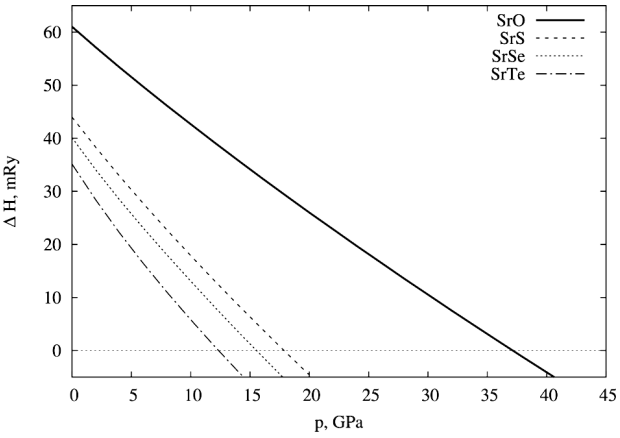

Fig. 2. Dependences of the enthalpy difference between strontium oxide and strontium chalcogenides on the pressure

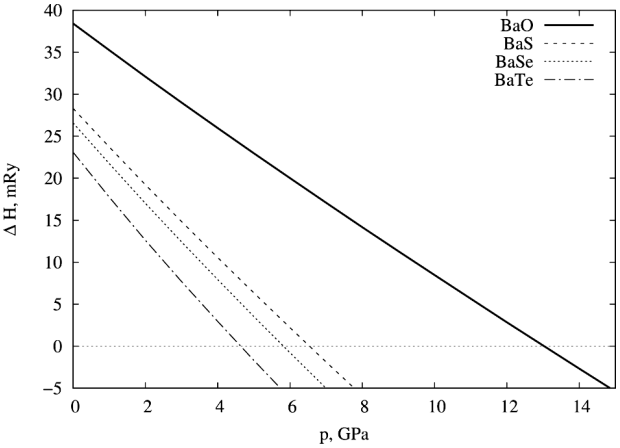

Fig. 3. Dependences of the enthalpy difference between barium oxide and barium chalcogenides on the pressure

at the phase transition

$$\Delta V_1 = \frac{V_{\rm pt}^{\rm B1} - V_{\rm pt}^{\rm B2}}{V_0^{\rm B1}}, \quad \Delta V_2 = \frac{V_{\rm pt}^{\rm B1} - V_{\rm pt}^{\rm B2}}{V_{\rm pt}^{\rm B1}}.$$

It should be noted that Table 3, as well as Tables 7 to 9 (see below), also contains the results of calculations for a hypothetical B1–B2 structural phase transition in BaO, which has not been detected experimentally.

The corresponding experimental results are presented in Table 4. The unit cell volume reductions were calculated in the cases where it was possible, and they were verified on the basis of data from other relevant works. Sometimes, it was not clear what quantity the cited authors meant as the unit cell volume reduction, which could give rise to certain inconsistencies in Table 4.

In Figs. 1 to 3, the dependences of the enthalpy difference on the pressures are shown for the AEMOCs: in Fig. 1 for calcium oxide CaO and calcium chalcogenides CaX, in Fig. 2 for strontium oxide SrO and strontium chalcogenides SrX, and in Fig. 3 for barium oxide BaO and barium chalcogenides BaX.

A comparison of the results of this work with the experimental data shows their quite reasonable agreement for the parameters of the B1–B2 phase transition in the AEMOCs. For example, for the phase transition pressure p_{pt}, the deviation is often appreciably below 10%. Exceptions are calcium chalcogenides (CaS, CaSe, CaTe) and SrSe, for which the deviations equal 10–12%. The results of the known theoretical works were obtained with different accuracies, and, sometimes, substantial deviations are noticeable. But, in most cases, our results are in reasonable agreement with the experimental data.

5. Dependence of the Size of the AEM, Oxygen, and Chalcogen Ions on the Pressure in the B1 and B2 Structures

The AEMOC compounds, as well as the alkali metal halogenides, are described rather well in the framework of the ion model. A lot of works concerning the properties of AEMOCs were performed in the framework of models that account for the ionic character of those compounds. The lattice of ionic crystals can be represented as alternating distributions of charges with different signs and close to spherical ones. In the simplest case, they can be represented as touching spheres with the corresponding radii. Such mod-

Table 5. **Distance between the nearest neighbors (in Å units) in AEMOCs in the B1 (upper values) and B2 (lower values) structures at various pressures**

p, GPa	CaO	CaS	CaSe	CaTe	SrO	SrS	SrSe	SrTe	BaO	BaS	BaSe	BaTe
0	2.42	2.86	2.98	3.20	2.60	3.03	3.15	3.36	2.73	3.18	3.30	3.51
	2.54	3.02	3.16	3.40	2.72	3.17	3.31	3.54	2.80	3.28	3.42	3.64
4.6325	2.38	2.79	2.90	3.09	2.56	2.95	3.06	3.24	2.68	3.09	3.19	3.37
	2.51	2.95	3.08	3.29	2.68	3.09	3.22	3.42	2.75	3.18	3.30	3.51
5.8165	2.38	2.78	2.89	3.07	2.55	2.93	3.04	3.21	2.67	3.07	3.17	3.34
	2.50	2.94	3.06	3.27	2.67	3.08	3.20	3.40	2.73	3.16	3.28	3.48
6.536	2.37	2.77	2.88	3.06	2.54	2.92	3.03	3.20	2.66	3.06	3.16	3.33
	2.50	2.93	3.05	3.26	2.66	3.07	3.19	3.38	2.73	3.15	3.27	3.46
12.348	2.34	2.71	2.81	2.98	2.50	2.86	2.95	3.11	2.61	2.98	3.08	3.23
	2.46	2.87	2.99	3.18	2.62	3.00	3.11	3.29	2.68	3.07	3.18	3.37
13.026	2.34	2.71	2.80	2.97	2.50	2.85	2.95	3.10	2.61	2.97	3.07	3.22
	2.46	2.87	2.98	3.17	2.62	3.00	3.10	3.28	2.67	3.07	3.18	3.36
15.549	2.33	2.69	2.78	2.94	2.49	2.83	2.92	3.07	2.59	2.95	3.04	3.19
	2.45	2.84	2.96	3.14	2.60	2.97	3.08	3.25	2.65	3.04	3.15	3.32
17.872	2.32	2.67	2.76	2.92	2.47	2.81	2.90	3.05	2.57	2.93	3.02	3.16
	2.44	2.83	2.94	3.12	2.59	2.95	3.05	3.23	2.64	3.02	3.12	3.29
29.190	2.27	2.60	2.68	2.83	2.42	2.73	2.81	2.95	2.51	2.84	2.93	3.06
	2.39	2.75	2.85	3.03	2.54	2.87	2.96	3.13	2.57	2.93	3.03	3.19
33.509	2.26	2.58	2.66	3.80	2.41	2.71	2.79	2.92	2.49	2.82	2.90	3.03
	2.38	2.73	2.83	3.00	2.52	2.85	2.93	3.10	2.55	2.90	3.00	3.15
36.103	2.25	2.57	2.65	2.78	2.40	2.70	2.77	2.90	2.48	2.80	2.88	3.01
	2.37	2.72	2.82	2.99	2.51	2.83	2.92	3.08	2.54	2.88	2.99	3.14
37.146	2.25	2.56	2.64	2.78	2.39	2.69	2.77	2.90	2.48	2.80	2.88	3.00
	2.36	2.71	2.81	2.98	2.51	2.83	2.91	3.07	2.53	2.88	2.98	3.13
65.238	2.18	2.47	2.53	2.65	2.31	2.58	2.65	2.77	2.38	2.68	2.75	2.87
	2.29	2.61	2.69	2.86	2.43	2.71	2.78	2.94	2.43	2.74	2.85	2.99

els have been known since the works by Wasastjerna, Goldschmidt, Zachariasen, and Pauling [24]. The corresponding radii of the spheres (the ionic radii) can be determined from crystallographic data, both experimental and theoretical, as well as by analyzing some other properties of solids (electronegativity, polarizability, ionicity, or the covalence degree). The processing of large arrays of crystallographic data was first implemented by Goldschmidt. Afterward, it was used in some other works (see, e.g., work [25]). Most of the models are based on a certain basic ionic radius R_{ion} inherent to a definite ion. The lattice modification under the pressure action raises an issue of the efficiency of such a model, if a compression of those ions together with a diminishing of the unit cell volume with the increasing pressure is possible. First, when being compressed, spherically symmetric distributions of the electron density become deformed and deviate more and more from the spherical symmetry. Second, both the ionic radius and the deformation depend on the coordination number at the compression. Therefore, either a correction for the coordination has to be taken into account or the values of ionic radii have to be considered depending on the

Table 6. **Ionic radii (in Å units) for AEMs, oxygen, and chalcogens at $p = 0$ (notations for ionic radii values are taken from work [24]: P stands for Pauling and G for Goldschmidt)**

Ion	Ionic radius								Crystalline radius					
	This work		[25]		[24]		[28]	[29]	This work		[25]		[30]	
	B1	B2	B1	B2	P	G	exp.	exp.	B1	B2	B1	B2	exp.	theor.
Ca^{2+}	1.02	1.12	1.00	1.12	0.99	1.06	1.08	1.06	1.16	1.26	1.14	1.26	1.32	1.28
Sr^{2+}	1.20	1.30	1.18	1.26	1.13	1.27	1.21	1.15	1.34	1.42	1.32	1.40	1.27	1.42
Ba^{2+}	1.33	1.38	1.35	1.42	1.35	1.43	1.43	1.29	1.47	1.52	1.49	1.56	1.49	1.61
O^{2-}	1.40	1.42	1.40	1.42	1.40	1.32	1.40		1.26	1.28	1.26	1.28		
S^{2-}	1.84	1.90	1.84		1.84	1.74	1.75		1.70	1.75	1.70			
Se^{2-}	1.96	2.04	1.98		1.98	1.91	1.87		1.82	1.90	1.84			
Te^{2-}	2.18	2.28	2.21		2.21	2.11	2.02		2.04	2.12	2.07			

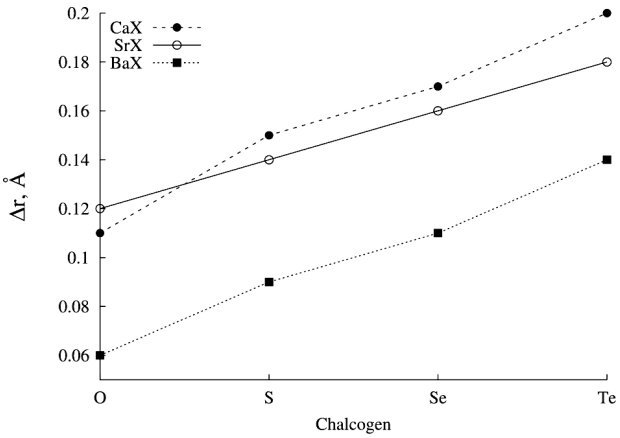

Fig. 4. Changes in the ionic radius at the B1–B2 phase transition in the AEMOCs

coordination, i.e. different values of ionic radii for different coordination numbers have to be introduced.

Fumi and Tosi [26, 27] have proposed to consider "crystalline radii", which are more physically substantiated and make allowance for the compression of ions in the crystal lattice. In the models used earlier, the radius of oxygen ion (as well as the radii of chalcogen ions) was overestimated, because it was taken the same as for an almost free oxygen ion. Accordingly, the radii of metal ions were underestimated. In works [26, 27], the ionic repulsion was proposed to be taken into account in the Born form, which led to a reasonable reduction in the radii of both oxygen and chalcogen ions.

The first-principles calculations allow the distances r between the nearest neighbors to be determined with a sufficient accuracy. Therefore, it is possible to determine the ionic radii in the B1 and B2 structures by neglecting a deformation under the compression and study their changes under the pressure action.

Thus, the set of initial data for calculations includes the calculation results for the distances r to the nearest neighbors in the B1 and B2 structures, which are quoted in Table 5 for pressures ranging from $p = 0$ to the phase transition pressure $p_{\rm pt}$ in CaO (it is the largest value among the phase transition pressures in the considered AEMOCs). Each intermediate pressure value in Table 5 corresponds to the phase transition in a definite AEMOC (see Table 3). So, at each pressure value from Table 5, there occur B1–B2 structural changes for one of the compounds, and, accordingly, the change in the distances to the nearest neighbors corresponds to this transition. Figure 4 demonstrates the changes of the distances to the nearest neighbors Δr at the phase transition within the CaX, SrX, and BaX series. Those dependences are linear with a high accuracy, being almost identical for the calcium and strontium chalcogenides.

In Table 6, the ionic and crystalline radii calculated in this paper in the framework of the first-principles approach are shown together with the results obtained by other authors. Our calculations were carried out under two assumptions: (i) according to work [25], the ionic and crystalline radii of the oxygen ion O^2 in the B1 and B2 phases are fixed; and (ii) the

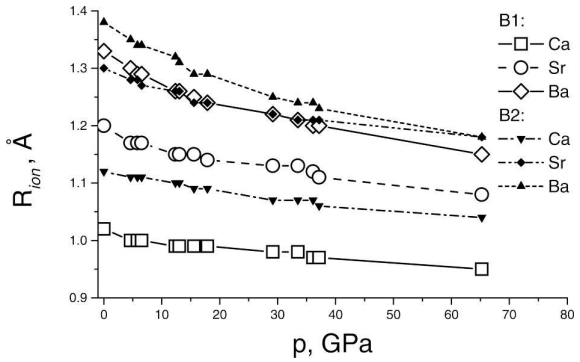

Fig. 5. Dependences of the ionic radii of AEMs on the pressure

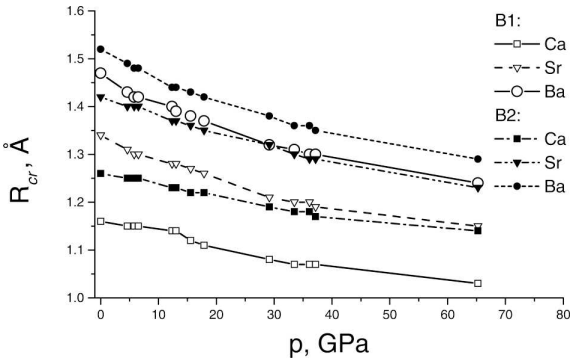

Fig. 6. Dependences of the crystalline radii of AEMs on the pressure

radii of other ions were obtained by minimizing the sum of squared deviations in the series of MeX compounds for AEMs, oxygen, and chalcogens, respectively. The calculated dependences of the ionic radii of the AEMs, oxygen, and chalcogens in the B1 and B2 structures on the pressure are depicted in Figs. 5 and 7, and the dependences of the crystalline radii of the ions of AEMs, oxygen, and chalcogens in the B1 and B2 structures on the pressure are shown in Figs. 6 and 8. The recalculation for larger pressure values was based on assumption (ii) and took into account that the compressibility of ionic radii is proportional to their values, both oxygen and chalcogen ions including.

The values of the ratio between the cation and anion ionic radii in the B1 structure at the zero and phase transition pressures and in the B2 structure under the phase transition and metallization pressures are quoted in Table 7. As the pressure in the B1 structure grows to the phase transition pressure, this ratio increases (except for BaO). At the phase transition to the B2 structure, it also increases (except for BaTe). If the pressure increases further to the metallization pressure, different compounds demonstrate different behavior of this ratio.

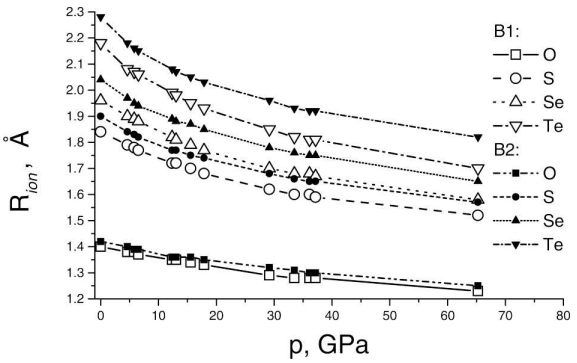

Fig. 7. Dependences of the ionic radii of oxygen and chalcogens on the pressure

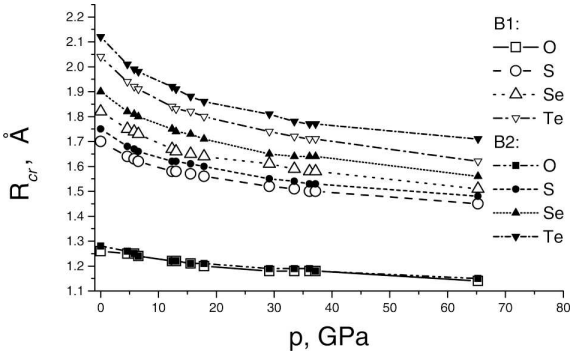

Fig. 8. Dependences of the crystalline radii of oxygen and chalcogens on the pressure

6. Interband Transitions and Forbidden Gaps in the B1 and B2 Structures of the AEMOCs

The results of calculations of gaps in the AEMOCs for the B1 structure are presented in Table 8. Hereafter, the following notations for the high-symmetry points in the B1 structure are used: Γ(0, 0, 0), X(1, 0, 0), L(0.5, 0.5, 0.5), W(1, 0.5, 0), U(1, 0.25, 0.25), and K(0.75, 0.75, 0) (in terms of $2\pi/a$ units). The values of the direct gaps Γ–Γ, X–X, and L–L are given at the pressures $p = 0$ and $p = p_{\rm pt}$. The minimum gaps (min gap) and their magnitudes obtained from the first-principles calculations of band structures in the framework of the DFT theory are also indicated. It should be noted that, as is known, those values are

underestimated in comparison with the corresponding experimental data.

In most cases, the minimum gaps correspond to indirect Γ–X transitions. Exceptions include BaO, for which the direct X–X transition was obtained in all calculations, and SrO and BaS, for which the minimum gap becomes the direct X–X gap at $p = p_{\rm pt}$.

For the B2 structure, the corresponding values are presented in Table 9. Namely, these are the direct gaps M—M, Γ–Γ, and X–X, the minimum gaps (min gap), and their values calculated for $p = p_{\rm pt}$. The minimum gaps are more diverse for the B2 structure of the AEMOCs. In particular, they include both the direct M–M and Γ–Γ transitions and the indirect Γ–M one. For the B2 structure, the following notations are used for the high-symmetry points: Γ(0, 0, 0), X(1, 0, 0), M(1, 1, 0), and R(1, 1, 1) (in terms of π/a units).

The result of DFT calculations for the CaTe compound in the B2 phase demonstrates the absence of gap at any pressure, which corresponds to the metallic state. The minimum gap also disappears at negative pressures, i.e. at volumes exceeding the equilibrium one, and it is the direct M–M gap. Hence, the calculated B1–B2 phase transition at 29.19 GPa (Table 3) is also an insulator-metal transition. The smallest $E_{\rm gap}$ is inherent to compounds in which the minimum $E_{\rm gap}$ corresponds to the direct M–M gap; these are CaSe, CaTe, and, perhaps, SrTe. Maybe, they have the most distorted band structures in this approach. The largest $E_{\rm gap}$ were calculated for compounds with the direct Γ–Γ gap (the AEM oxides CaO, SrO, and BaO, as well as BaS).

The experimental results for the B1 phase are gathered in Table 10. Table 11 contains known results, both experimental and theoretical, for the B2 structure. The abbreviations used in Table 11 to denote the applied calculation methods are as follows: exp. stands for experimental results, TB LMTO for

Table 7. **Ratio between the cation and anion ionic radii in the B1 and B2 structures in AEMOCs at various pressures: zero ($p = 0$), phase transition ($p = p_{\rm pt}$), and metallization ($p = p_{\rm met}$)**

Compound	B1		B2	
	$p = 0$	$p = p_{\rm pt}$	$p = p_{\rm pt}$	$p = p_{\rm met}$
CaO	0.729	0.744	0.817	0.940
CaS	0.554	0.606	0.649	0.648
CaSe	0.520	0.583	0.608	0.600
CaTe	0.468	0.530	0.546	0.491
SrO	0.857	0.867	0.931	0.910
SrS	0.652	0.679	0.713	0.748
SrSe	0.612	0.643	0.663	0.686
SrTe	0.551	0.578	0.606	0.605
BaO	0.950	0.933	0.963	0.908
BaS	0.723	0.729	0.736	0.742
BaSe	0.679	0.683	0.687	0.705
BaTe	0.610	0.625	0.619	0.633

Table 8. **Calculated values (in eV units) of the gaps at high-symmetry points and the minimum gap for the B1 structure in the AEMOCs at zero pressure and at the corresponding phase transition pressure**

Compound	Pressure	Γ–Γ	X–X	L–L	min gap	$E_{\rm gap}^{\rm min}$
CaO	0	4.6050	4.0308	8.1400	X–Γ	3.6537
	$p_{\rm pt}$	6.8256	3.5304	10.4395	X–Γ	3.3298
CaS	0	4.1017	3.1860	6.3322	X–Γ	2.3871
	p_{pt}	3.8037	2.2854	7.6795	X–Γ	1.2942
CaSe	0	3.5165	2.9515	5.6503	X–Γ	2.0391
	$p_{\rm pt}$	3.1597	1.9912	6.9712	X–Γ	0.7534
CaTe	0	2.9658	2.6174	4.7840	X–Γ	1.5539
	$p_{\rm pt}$	2.2114	1.6667	5.9811	X–Γ	0.0437
SrO	0	3.7665	3.4238	7.4911	X–Γ	3.3187
	$p_{\rm pt}$	5.7751	2.9112	9.1690	X–X	2.9112
SrS	0	3.5639	2.9791	6.3586	X–Γ	2.5143
	$p_{\rm pt}$	4.2724	2.3588	7.3882	X–Γ	1.9082
SrSe	0	3.1078	2.7817	10.3691	X–Γ	2.2133
	$p_{\rm pt}$	3.7509	2.1633	13.0590	X–Γ	1.5449
SrTe	0	2.7099	2.4868	4.8735	X–Γ	1.7669
	$p_{\rm pt}$	2.9639	1.8947	5.6191	X–Γ	1.0156
BaO	0	4.5844	1.9777	6.6912	X–X	1.9777
	$p_{\rm pt}$	5.8354	1.3580	7.5384	X–X	1.3580
BaS	0	3.8719	2.3719	6.5038	X–Γ	2.3179
	p_{pt}	4.1403	2.0745	6.9628	X–X	2.0745
BaSe	0	3.4293	2.2320	5.9219	X–Γ	2.0732
	$p_{\rm pt}$	3.7091	1.9343	6.3477	X–Γ	1.8668
BaTe	0	3.0091	2.0142	5.1011	X–Γ	1.6937
	$p_{\rm pt}$	3.0381	1.7216	5.4414	X–Γ	1.4395

Table 9. **Calculated values (in eV units) of the gaps at high-symmetry points and the minimum gap for the B2 structure in the AEMOCs at the corresponding phase transition pressure and parameters of AEMOC metallization**

Compound	M–M	Γ–Γ	X–X	min gap	$E_{\text{gap}}^{\text{min}}$	met	p_{met}, GPa	V_{met}/V_0
CaO	4.5444	2.6873	5.0897	Γ–M	2.5084	Γ–Γ	505	0.400
CaS	0.7784	1.2435	2.6433	Γ–M	0.3210	Γ–M	48.8	0.624
CaSe	–0.0931	0.9072	3.1157	M–M	–0.931	M–M	$25.5<p_{\text{pt}}$	0.692
CaTe	<0	<0	<0	M–M	<0	M–M	$(<0)<p_{\text{pt}}$	0.925
SrO	4.9342	2.5567	5.0361	Γ–Γ	2.5567	Γ–Γ	368	0.415
SrS	1.7795	1.6262	3.9278	Γ–M	1.2044	Γ–M	69.5	0.547
SrSe	1.0415	1.3485	3.4593	Γ–M	0.7562	Γ–M	34	0.618
SrTe	0.0061	0.9993	2.7466	M–M	0.0061	M–M	13.5	0.712
BaO	4.8651	1.8691	4.4730	Γ–Γ	1.8691	Γ–Γ	129	0.455
BaS	2.6794	1.3804	3.4754	Γ–Γ	1.3804	Γ–Γ	44	0.549
BaSe	2.0211	1.1746	3.0522	Γ–M	1.1639	Γ–Γ	35	0.573
BaTe	1.0894	0.9003	2.5427	Γ–M	0.6405	Γ–M	22	0.611

the tight-binding linear muffin-tin orbital method, DFT for the density functional theory method, LDA for the local density approximation method, GGA for the generalized gradient approximation method, APW for the augmented plane wave method, ASW for the augmented spherical wave method, GW for the GW approximation method, EV for the Engel–Vosko scheme, FP-LAPW for the full-potential linearized augmented plane wave method, and FP-PW for the full-potential plane wave approach.

7. Pressure-Induced Metallization of AEM Chalcogenides

The results of first-principles calculations of the band structure in the AEMOCs confirm the metallization of those compounds at high pressures. This conclusion follows from the analysis of the dependence of the gap magnitude on the pressure. The above-mentioned underestimation of the relevant values in the DFT approach may also result in the underestimation of the metallization pressure value p_{met}. Table 9 demonstrates the metallization pressure values obtained in such calculations, as well as the relative metallization volume V_{met}/V_0 (with respect to to the equilibrium volume in the B1 structure), and the magnitudes of the gap that disappears at the metallization.

It should be noted that, in addition to CaTe, the CaSe compound also has a specific feature: the corresponding calculated values are $p_{\text{met}} = 25.5$ GPa

Table 10. **Experimental interband transitions (in eV units), minimum gaps and their magnitude (in eV units) in AEMOCs in the B1 structure**

Compound	Γ–Γ	X–X	L–L	min gap	$E_{\text{gap}}^{\text{min}}$	Source
CaO	7.03	7.3	9.5	Γ–X	6.79	[31]
				Γ–X	7.03	[32]
				Γ–X	7.08	[33]
	7.085	7.46	7.16			[34]
		6.875				[35]
	16.5					[36]
CaS	5.80	5.343		Γ–X	4.434	[35]
CaSe		4.898		Γ–X	3.85	[35]
SrO	5.896	6.28	5.97	Γ–Γ	5.896	[34]
	6.08	5.79				[35]
SrS	5.387	4.831		Γ–X	4.32	[35]
SrSe	4.570	4.475		Γ–X	3.813	[35]
BaO	8.3	3.985				[35]
					3.88	[37]
					4.10	[38]
BaS	5.229	3.941		Γ–X	3.806	[35]
					3.88	[37]
					3.90	[38]
BaSe	4.556	3.658		Γ–X	3.421	[35]
					3.58	[37]
					3.60	[38]
BaTe					3.08	[37]
					3.10	[38]

Table 11. **Experimental interband transitions (in eV units), minimum gaps and their magnitude (in eV units) in AEMOCs in the B2 structure**

Compound	M–M	Γ–Γ	X–X	min gap	$E_{\text{gap}}^{\text{min}}$	p_{met}, GPa	V_{met}, Å^3	V_{met}/V_0	Method	Source
CaO				M–Γ	2.3				TB LMTO	[39]
					2.1	480			LDA + APW	[40]
CaS		1.35		Γ–Γ	1.35				GGA	[41]
		2.06		Γ–Γ	2.06	85.07		0.602	GGA-EV	[41]
CaSe					0.97–0.81	>125			exp.	[42]
					0.65				DFT + GW	[42]
	0.79			M–M	0.79				GGA	[41]
	1.49			M–M	1.49	54.01		0.655	GGA-EV	[41]
						36.03	36.0	0.690	FP-LAPW	[43]
CaTe	0.007			M–M	0.00728				GGA	[41]
	0.55			M–M	0.55	39.87		0.834	GGA-EV	[41]
						35.48	41.06	0.622	FP-LAPW	[44]
SrO				M–Γ	2.4				TB LMTO	[39]
SrS						90		0.53	exp.	[12]
						54		0.59	TB LMTO	[45]
						69	30.90	0.551	FP-LAPW	[46]
						63.3			GGA	[47]
		2.11	3.72	M–Γ	1.83				GGA	[48]
SrSe						24		0.656	TB LMTO	[45]
						41	37.94	0.600	FP-LAPW	[46]
SrTe						18		0.688	TB LMTO	[45]
						14	55.00	0.712	FP-LAPW	[46]
BaO						100			exp.	[17]
BaS						62.2		0.55	exp.	[17]
					1.6–1.35	>113			exp.	[42]
						47	37.93	0.564	FP-LAPW	[44]
						49.1		0.574	TB LMTO	[49]
					1.46				DFT + GW	[50]
						32		0.60	ASW	[51]
						32		0.62	ASW	[51]
BaSe						52		0.555	exp.	[52]
						31		0.625	TB LMTO	[49]
						31.5		0.61	LAPW	[53]
						17		0.63	ASW	[51]
						17		0.66	ASW	[51]
BaTe						20		0.65	exp.	[20]
						<27		>0.62	exp.	[54]
						<100		0.71	LMTO	[54]
						14.1		0.684	TB LMTO	[49]
						15.8		0.67	LAPW	[19]
						19.54		0.66	FP-LAPW–GGA	[55]
						27.55		0.54	FP-PW–GGA	[55]
						19.29		0.55	FP-PW–LDA	[55]
						40		0.74	ASW	[51]
						40		0.77	ASW	[51]

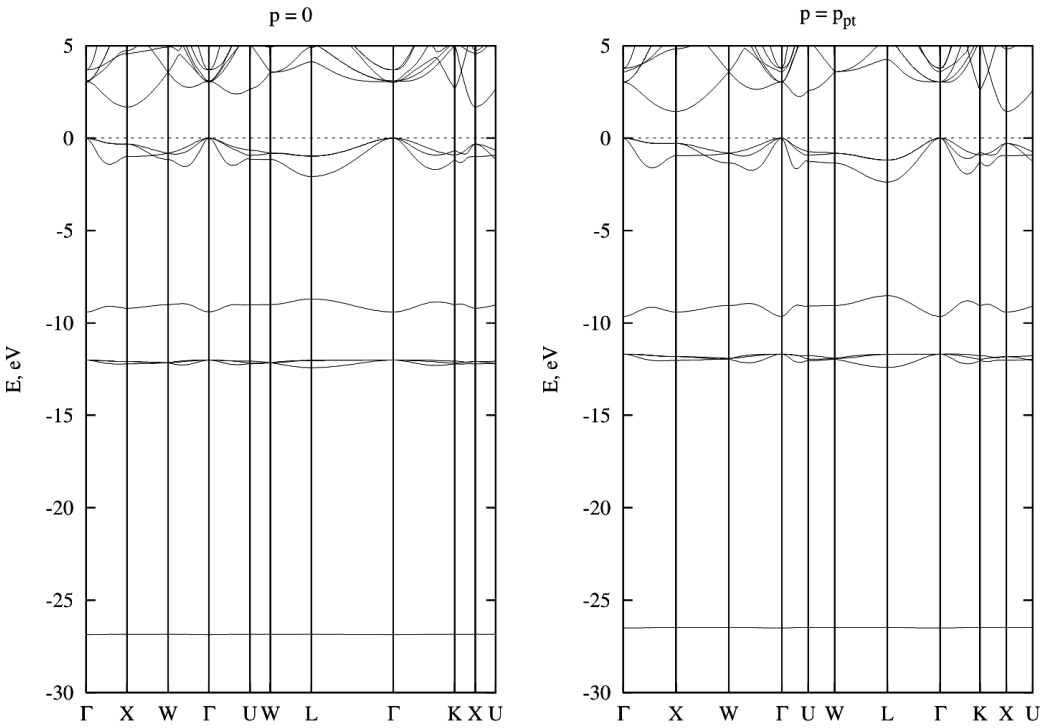

Fig. 9. Band structure of BaTe in the B1 phase

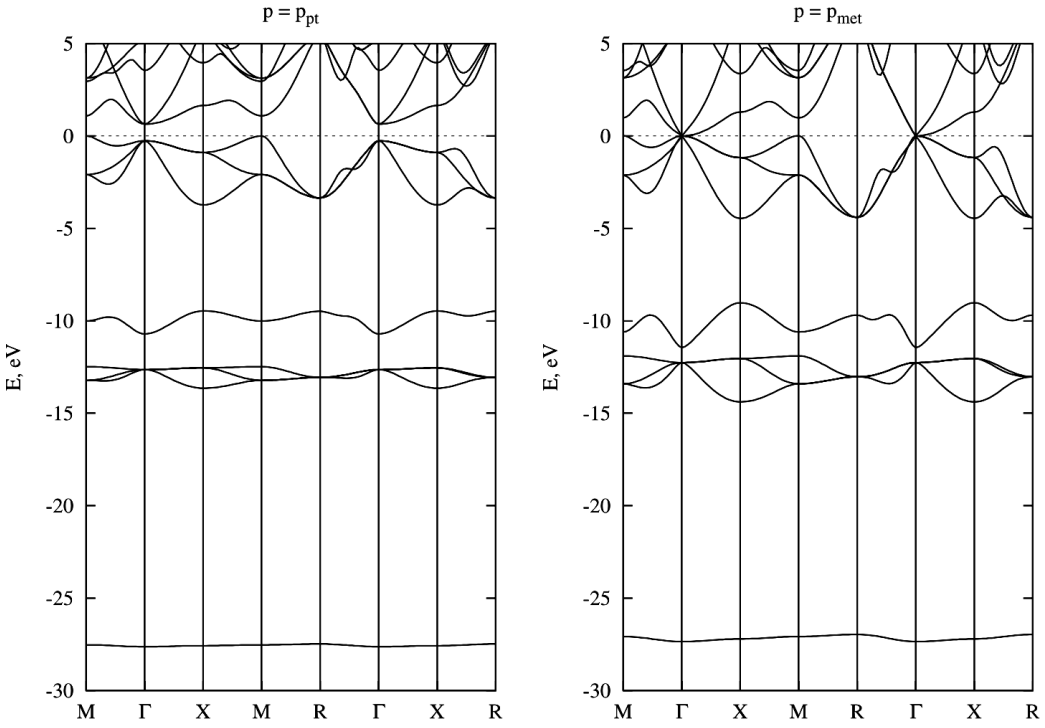

Fig. 10. Band structure of BaTe in the B2 phase

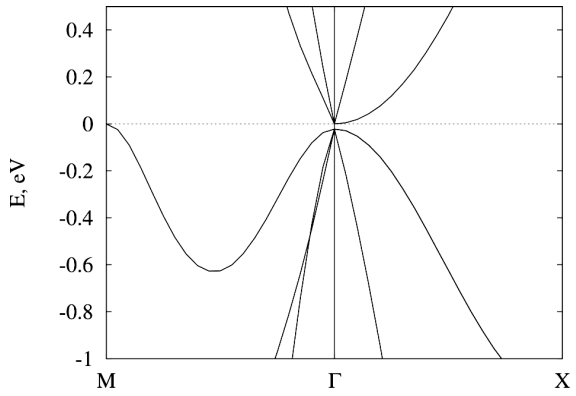

Fig. 11. Fragment of the band structure of BaTe in the B2 phase at the metallization pressure

and $p_{\rm pt} = 33.509$ GPa. In other words, according to the results of first-principles calculations made of this work, the B1–B2 transition has to be accompanied by the insulator-metal phase transition. Perhaps, the absence of the gap in CaTe at $p = 0$ in the B2 structure may testify to the incorrectness of the first-principles results obtained in this work for this compound.

At the metallization of the CaO and BaSe compounds, the gap undergoes changes: it transforms from the indirect gap Γ–M to the direct one Γ–Γ. In other AEMOCs, the minimum gaps do not vary when changing from the phase transition pressure to the metallization pressure. The largest values of the pressure $p_{\rm met}$ were obtained for the AEM oxides, in which the gap is the direct gap Γ–Γ.

The values of the parameters that characterize the metallization transition in the AEMOCs, which were determined in other works, are gathered in Table 11. The B2 phase was considered in very few experimental works. A comparison with the results of experimental works points to a very low value of $p_{\rm met}$ calculated for CaSe, its appreciable underestimation for BaS (moreover, for this compound, various experimental data differ substantially from one another) and BaSe, and good agreement for BaTe. The available experimental data for the metallization volume $V_{\rm met}$ agree well with the results of this work obtained for BaS, BaSe, and BaTe. Sometimes there is no agreement with the results of other theoretical works, namely, for CaS, CaSe, and CaTe, maybe because of the lack of relevant experimental data. For other compounds, the results of this work are in good agreement with the results of calculations by other authors.

Theoretical calculations may be quite different in detail, but they provide results comparable with the experiment. As an example, let us consider the results of calculations for experimentally well-studied barium telluride. The values obtained for the metallization volumes and pressures of BaTe are comparable with one another and with the experimental data. Figures 9 and 10 demonstrate the band structures in the B1 and B2 phases of BaTe at different pressures, which were found in this work and which can be compared with their counterparts found in works [49, 55]. The band structures reveal a similar behavior at the zero pressure and the phase transition pressure. But the results of works [49, 55] clearly demonstrate that it is the indirect transition Γ–M that undergoes the metallization at the metallization pressure. From Fig. 10, it may seem that the metallization occurs at the direct transition Γ–Γ. However, Fig. 11 illustrates a scaled-up fragment of the BaTe band structure at the metallization pressure, whence one can clearly see that the metallization occurs at the indirect transition Γ–M.

8. Conclusions

In this paper, the results of the first-principles DFT-based calculations of the thermodynamic parameters of the AEMOCs in the B1 and B2 structures have been reported in order to illustrate the application scheme of this approach while studying the properties of AEMOCs subjected to the pressure action. The following results were obtained and the following conclusions can be drawn.

1. Modern methods applied for the calculation of the equilibrium structural properties of crystalline structures can reproduce the structural characteristics of the AEMOCs with a sufficient accuracy. The corresponding calculation of the parameters of the B1–B2 phase transition in the AEMOCs brings about results that are in good agreement with the experimental data.

2. The calculated interband transitions turn out underestimated, if they are calculated in the DFT framework. At the same time, there are methods, e.g., the Hartree–Fock approximation, that substantially overestimate those parameters. There are few experimental data for the AEMOCs in the B2 structure. This fact does not allow appropriate comparisons to be made in most cases.

3. The change of the ionic radii of the AEM atoms, oxygen, and chalcogens under pressure in the B1 and B2 structures was found. The ratio between the cation and anion ionic radii increases with the pressure: first, at pressures up to the B1–B2 phase transition pressure; then, directly at the phase transition. Such a behavior is not observed near the metallization pressure p_{met}.

4. The metallization pressure values p_{met} were calculated for the AEMOCs in the B2 structure. The results obtained were found to be underestimated in comparison with the experimental data, but they agree with the results of other theoretical works.

5. For some compounds (CaSe, CaTe), the first-principles calculation of the band structure carried out in this work leads to a premature disappearance of the band gap and a substantial reduction of the metallization pressure.

1. P. Hohenberg, W. Kohn. Inhomogeneous electron gas. *Phys. Rev.* **136**, 864 (1964).
2. P. Giannozzi, S. Baroni, M. Calandra, R. Car, C. Cavazzoni, D. Ceresoli, G.L. Chiarotti, M. Cococcioni, I. Dabo, A. Dal Corso, S. Fabris, G. Fratesi, S. de Gironcoli, R. Gebauer, U. Gerstmann, Ch. Gougoussis, A. Kokalj, M. Lazzeri, L. Martin-Samos, N. Marzari, F. Mauri, R. Mazzarello, S. Paolini, A. Pasquarello, L. Paulatto, C. Sbraccia, S. Scandolo, G. Sclauzero, A.P. Seitsonen, A. Smogunov, P. Uniari, R.M. Wentzcovitch. QUANTUM ESPRESSO: a modular and open-source software project for quantum simulations of materials. *J. Phys.: Condens. Matter* **21**, 395502 (2009).
3. J.P. Perdew, K. Burke, M. Ernzerhof. Generalized gradient approximation made simple. *Phys. Rev. Lett.* **77**, 3865 (1996).
4. D. Vanderbilt. Soft self-consistent pseudopotentials in a generalized eigenvalue formalism. *Phys. Rev. B* **41**, 7892 (1990).
5. A.M. Rappe, K.M. Rabe, E. Kaxiras, J.D. Joannopoulos. Optimized pseudopotentials. *Phys. Rev. B* **41**, 1227 (1990).
6. A.M. Rappe, K.M. Rabe, E. Kaxiras, J.D. Joannopoulos. Erratum: Optimized pseudopotentials. *Phys. Rev. B* **44** 13175 (1991).
7. F. Birch. Finite strain isotherm and velocities for single-crystal and polycrystalline NaCl at high pressure and 300 K. *J. Geophys. Res.* **83**, 1257 (1978).
8. H.J. Monkhorst, J.D. Pack. Special-points for Brillouin-zone integrations. *Phys. Rev. B* **13**, 5188 (1976).
9. P. Richet, H.K. Mao, P.M. Bell. Static compression and equation of state of CaO to 1.35 Mbar. *J. Geophys. Res.* **93**, 15279 (1988).
10. H. Luo, R.G. Green, K. Ghandehari, T. Li, A.L. Ruoff. Structural phase transformations and the equations of state of calcium chalcogenides at high pressure. *Phys. Rev. B* **50**, 16232 (1994).
11. L.G. Liu, W.A. Bassett. Changes of the crystal structure and the lattice parameter of SrO at high pressure. *J. Geophys. Res.* **78**, 8470 (1973).
12. K. Syassen. Pressure-induced structural transition in SrS. *Phys. Status Solidi A* **91**, 11 (1985).
13. H. Luo, R.G. Greene, A.L. Ruoff. High-pressure phase transformation and the equation of state of SrSe. *Phys. Rev. B* **49**, 15341 (1994).
14. H.G. Zimmer, H. Winzen, K. Syassen. High-pressure phase transitions in CaTe and SrTe. *Phys. Rev. B* **32**, 4066 (1985).
15. L.G. Liu, W.A. Bassett. Effect of pressure on the crystal structure and the lattice parameters of BaO. *J. Geophys. Res.* **77**, 4934 (1972).
16. S. Yamaoka, O. Shimomura, H. Nakazawa, O. Fukunaga. Pressure-induced phase transformation in BaS. *Solid State Commun.* **33**, 87 (1980).
17. S.T. Weir, Y.K. Vohra, A.L. Ruoff. High-pressure phase transitions and the equations of state of BaS and BaO. *Phys. Rev. B* **33**, 4221 (1986).
18. Y. Kaneko, K. Morimoto, T. Koda. Optical properties of alkaline-earth chalcogenides. I. Single crystal growth and infrared reflection spectra due to optical phonons. *J. Phys. Soc. Japan* **51**, 2247 (1982).
19. T.A. Grzybowski, A.L. Ruoff. High-pressure phase transition in BaSe. *Phys. Rev. B* **27**, 6502 (1983).
20. T.A. Grzybowski, A.L. Ruoff. Band-overlap metallization of BaTe. *Phys. Rev. Lett.* **53**, 489 (1984).
21. J.F. Mammone, H.K. Mao, P.M. Bell. Equations of state of CaO under static pressure conditions. *Geophys. Res. Lett.* **8**, 140 (1981).
22. R. Jeanloz, T.J. Ahrens, H.K. Mao, P.M. Bell. B1-B2 transition in calcium oxide from shock-wave and diamond-cell experiments. *Science* **206**, 829 (1979).
23. Y. Sato, R. Jeanloz. Phase transition in SrO. *J. Geophys. Res. B* **86**, 11773 (1981).
24. L. Pauling. *The Nature of the Chemical Bond* (Cornell Univ. Press, 1960).
25. R.D. Shannon. Revised effective ionic radii and systematic studies of interatomic distances in halides and chalcogenides. *Acta Cryst. A* **32**, 751 (1976).
26. F.G. Fumi, M.P. Tosi. Ionic sizes and born repulsive parameters in the NaCl-type alkali halides—I: The Huggins-Mayer and Pauling forms. *J. Phys. Chem. Solids* **25**, 31 (1964).
27. F.G. Fumi, M.P. Tosi. Ionic sizes and born repulsive parameters in the NaCl-type alkali halides—II: The generalized Huggins-Mayer form. *J. Phys. Chem. Solids* **25**, 45 (1964).
28. I.M. Boswarva. Ionic radii in the alkaline earth chalcogenides. *J. Phys. C* **1**, 582 (1968).
29. S. Israel, R. Saravanan, N. Srivasan, S.K. Mohanlal. An investigation on the bonding in MgO, CaO, SrO and BaO

from the MEM electron density distributions. *J. Phys. Chem. Solids* **64**, 879 (2003).
30. G. Vidal-Valat, J.P. Vidal, K. Kurki-Suonio. X-ray study of the atomic charge densities in MgO, CaO, SrO and BaO. *Acta Cryst. A* **34**, 594 (1978).
31. R.C. Whited, W.C. Walker. Exciton and interband spectra of crystalline CaO. *Phys. Rev.* **188**, 1380 (1969).
32. R.C. Whited, W.C. Walker. Exciton spectra of CaO and MgO. *Phys. Rev. Lett.* **22**, 1428 (1969).
33. R.C. Whited, Ch.J. Flaten, W.C. Walker. Exciton thermoreflectance of MgO and CaO. *Solid State Commun.* **13**, 1903 (1973).
34. A.S. Rao, R.J. Kearney. Logarithmic derivative reflectance spectra of BaO and SrO. *Phys. Status Solidi B* **95**, 243 (1979).
35. Y. Kaneko, T. Koda. New developments in IIa-VIb (alkaline-earth chalcogenide) binary semiconductors. *J. Cryst. Growth* **86**, 72 (1988).
36. M.A. Bolorizadeh, V.A. Sashin, A.S. Kheifets, M.J. Ford. Electronic band structure of calcium oxide. *J. Electr. Spectrosc. Rel. Phenom.* **141**, 27 (2004).
37. R.J. Zollweg. Optical absorption and photoemission of barium and strontium oxides, sulphides, selenides, and tellurides. *Phys. Rev.* **111**, 113 (1958).
38. G.A. Saum, E.B. Hensley. Fundamental optical absorption in the IIA–VIB compounds. *Phys. Rev.* **113**, 1019 (1959).
39. G. Kalpana, B. Palanivel, M. Rajagopalan. Electronic and structural properties of alkaline-earth oxides under high pressure. *Phys. Rev. B* **52**, 4 (1995).
40. J. Hama, M. Watanabe. Equation of state and electronic structure of solid CaO under high pressure. *Phys. Lett. A* **115**, 287 (1986).
41. Z. Charifi, H. Baaziz, F. El Haj Hassan, N. Bouarissa. High pressure study of structural and electronic properties of calcium chalcogenides. *J. Phys.: Condens. Matter* **17**, 4083 (2005).
42. Ph. Cervantes, Q. Williams, M. Côté, M. Rohlfing, M.L. Cohen, S.G. Louie. Band structures of CsCl-structured BaS and CaSe at high pressure: Implications for metallization pressures of the alkaline earth chalcogenides. *Phys. Rev. B* **58**, 9793 (1998).
43. R. Pandey, Ph. Lepak, J.E. Jaffe. Electronic structure of alkaline-earth selenides. *Phys. Rev. B* **46**, 4976 (1992).
44. R. Khenata, M. Sahnoun, H. Baltache, M. Rérat, D. Rached, M. Driz, B. Bouhafs. Structural, electronic, elastic and high-pressure properties of some alkaline-earth chalcogenides: An ab initio study. *Physica B* **371**, 12 (2006).
45. I.B.S. Banu, M. Rajagopalan, B. Palanivel, G. Kalpana, P. Shenbagaraman. Structural and electronic properties of SrS, SrSe, and SrTe under pressure. *J. Low Temp. Phys.* **112**, 211 (1998).
46. R. Khenata, H. Baltache, M. Rérat, M. Driz, M. Sahnoun, B. Bouhafs, B. Abbar. First-principle study of structural, electronic and elastic properties of SrS, SrSe and SrTe under pressure. *Physica B* **339**, 208 (2003).
47. L.-Y. Lu, J.-J. Tan, O.-H. Jia, X.-R. Chen. Transition phase and electronic structure of SrS under pressure from first-principles calculations. *Physica B* **399**, 66 (2007).
48. Ş. Uğur. Theoretical study of the phonon properties of SrS. *Mater. Sci. Eng. B* **162**, 116 (2009).
49. G. Kalpana, B. Palanivel, M. Rajagopalan. Electronic structure and structural phase stability in BaS, BaSe, and BaTe. *Phys. Rev. B* **50**, 12318 (1994).
50. E.V. Stepanova, V.S. Stepanyuk, M.N. Rogaleva, O.V. Farberovich, A.A. Grigorenko, V.V. Mikhailin. Electronic structure and optical properties of the CaO compound. *Fiz. Tverd. Tela* **30**, 2303 (1988) (in Russian).
51. A.E. Carlsson, J.W. Wilkins. Band-overlap metallization of BaS, BaSe, and BaTe. *Phys. Rev. B* **29**, 5836 (1984).
52. S.T. Weir, Y.K. Vohra, A.L. Ruoff. Pressure-induced metallization of BaSe. *Phys. Rev. B* **35**, 874 (1987).
53. S.-H. Wei, H. Krakauer. Local-density-functional calculation of the pressure-induced metallization of BaSe and BaTe. *Phys. Rev. Lett.* **55**, 1200 (1985).
54. K. Syassen, N.E. Christensen, H. Winzen, K. Fischer, J. Evers. Optical response and band-structure calculations of alkaline-earth tellurides under pressure. *Phys. Rev. B* **35**, 4052 (1987).
55. H. Akbarzadeh, M. Dadsetani, M. Mehrani. Electronic and structural properties of BaTe *Comp. Mater. Sci.* **17**, 81 (2000).

Received 20.05.19.
Translated from Ukrainian by O.I. Voitenko

В.В. Поживатенко

ІОННИЙ ХАРАКТЕР, ФАЗОВІ ПЕРЕХОДИ ТА МЕТАЛІЗАЦІЯ В ОКСИДАХ І ХАЛЬКОГЕНІДАХ ЛУЖНОЗЕМЕЛЬНИХ МЕТАЛІВ ПІД ТИСКОМ

Р е з ю м е

Виходячи з перших принципів, проведено розрахунки структурних і термодинамічних властивостей оксидів і халькогенідів лужноземельних металів, що мають кубічні структури (CaX, SrX, BaX, де X = O, S, Se, Te), а також характеристик структурних фазових переходів B1–B2 в цих речовинах під тиском. Досліджено кристалічні і іонні радіуси в оксидах і халькогенідах лужноземельних металів, у тому числі розглянуто залежність радіусів іонів в структурах B1 та B2 від тиску. Обчислено величини міжзонних переходів і заборонених зон в даних сполуках у підході теорії функціонала густини сумісно з методом псевдопотенціалу. В результаті зонних розрахунків знайдено значення тисків металізації в цих сполуках.